

LETTER • OPEN ACCESS

Crack and pull-off dynamics of adhesive, viscoelastic solids

To cite this article: Martin H. Müser and Bo N. J. Persson 2022 EPL 137 36004

View the article online for updates and enhancements.

You may also like

- Cleaning Process Applicable to Silicon Carbide Chemical Vapor Deposition

Hitoshi Habuka, Yusuke Fukumoto, Kosuke Mizuno et al.

- Hydrodynamic binary coalescence of droplets under air flow in a hydrophobic microchannel

Chao Wang, , Chao-qun Shen et al.

- Development of a robust fabrication process for single silicon nanowire-based omega gate transistors on polyamide substrate
T Arjmand, M Legallais, T Haffner et al.

EPL, **137** (2022) 36004

doi: 10.1209/0295-5075/ac535c

www.epljournal.org

Crack and pull-off dynamics of adhesive, viscoelastic solids

MARTIN H. MÜSER^{1(a)} ond Bo N. J. Persson^{2,3}

received 21 October 2021; accepted in final form 9 February 2022 published online 22 April 2022

Abstract – When quickly detaching an elastomer from a counterface, viscoelasticity dramatically increases the perceived adhesion relative to its adiabatic or equilibrium value. Here, we report simulations on the sticking contact between a rigid cylinder and a viscoelastic half space revealing a maximum in the work of separation at intermediate pull-off velocities. Maximum tensile forces yet increase monotonically with the pull-off speed and the crack tip speed in accordance with the Persson-Brener approach. As predicted theoretically, the fracture mode transitions from interfacial crack propagation to quasi-uniform bond breaking with increasing range of adhesion.



Copyright © 2022 The author(s)

Published by the EPLA under the terms of the <u>Creative Commons Attribution 4.0 International License</u> (CC BY). Further distribution of this work must maintain attribution to the author(s) and the published article's title, journal citation, and DOI.

Introduction. – We all know since childhood that the pain experienced when tearing off a bandage is small when pulling either very slowly or very quickly. In between these two limits, it hurts. One important reason for this phenomenon certainly is that breaking an adhesive, viscoelastic interface is crucially affected by the interplay of the interfacial energy, the maximum tension of the media in contact, the frequency dependence of their mechanical properties, and the pull-off velocity [1,2]. Similar comments can be made about the rupture and wear of rubber [3,4] as well as the adhesion, cohesion, and friction involving related elastomers including, for example, pressure-sensitive adhesives [5], tapes [6], or cartilage [7]. Unfortunately, even the most elementary linearly viscoelastic, adhesive interfaces (for which fibrillation, cavitation, and other complex phenomena that matter for the bandage example [4,5] can be neglected) defy a simple description of their dynamics.

The critical quantity in a viscoelastic fracture problem is the energy release rate G(v). It is the energy per unit area needed to advance a crack by a unit length as a function of the crack tip speed v. Traditionally [1,8–14], it is attempted to determine G(v) by solving a self-consistent equation, which first needs to be derived for each combination of a given frequency-dependent elastic modulus $E(\omega)$ and cohesive-zone model (CZM). The latter states how

adhesive stress changes locally with the interfacial separation, or gap q. However, as pointed out by de Gennes [15], certain universal features should apply given that the stress near crack tips generally obeys $\sigma(r) = K/\sqrt{2\pi r}$, a distance r away from the crack tip [16], where K is called the stress-intensity factor, see also fig. 1(c) —other panels of that figure are discussed in the model section, while mathematical symbols are summarized in table 1. In the immediate vicinity of a fast moving crack and very far away from it, the contact mechanics is similar to that of an adiabatically moving crack, however, assuming the highand low-frequency elastic modulus, E_1 and E_0 , at small and large r, respectively. Unfortunately, the interesting, non-trivial intermittent region is where most energy can be dissipated, whereby this region may predominantly account for the increase of G(v) compared to its quasi-static or adiabatic value G_0 .

Almost two decades ago, Persson and Brener [17] suggested an approximate solution for a broad class of viscoelastic, adhesive contact problems. A central benefit of their approach is that a relatively simple self-consistent integral equation needs to be solved, in which $E(\omega)$ can be arbitrarily complex without obstructing the calculation of G(v). It yet yields a similar speed dependence of the fracture energy as that determined from traditional solutions [11,13,18] of simple rheological models.

Neither the traditional nor the Persson-Brener approach have so far been verified by rigorous numerical solutions

¹ Dept. of Materials Science and Engineering, Saarland University - 66123 Saarbrücken, Germany

² PGI-1, FZ Jülich - Jülich, Germany

³ Multiscale Consulting - Wolfshovener Str. 2, 52428 Jülich, Germany

⁽a) E-mail: martin.mueser@mx.uni-saarland.de (corresponding author)

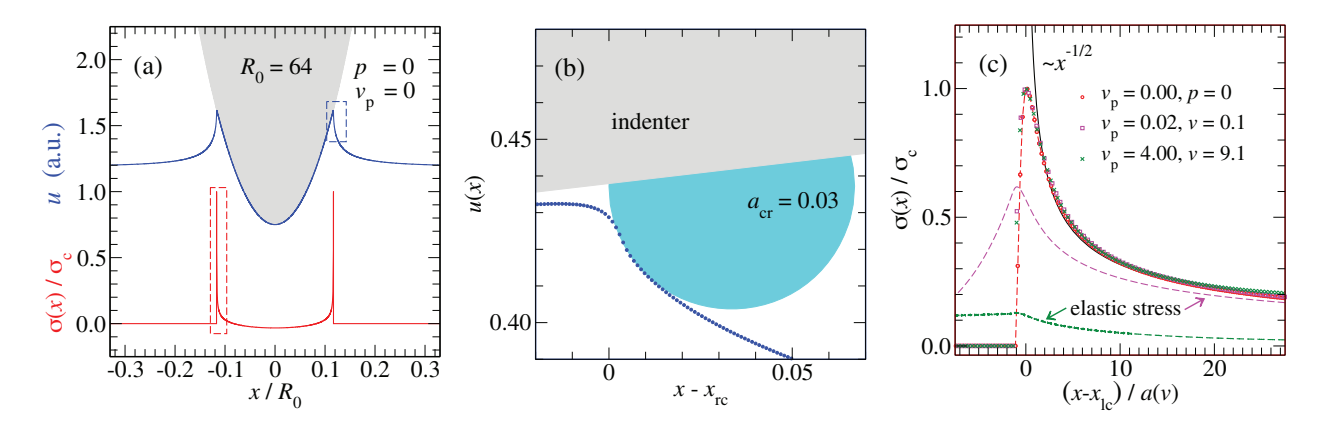


Fig. 1: (a) Displacement field u(x) (blue) and interfacial stress $\sigma(x)$ (red) in units of the maximum stress σ_c for the system with a contact radius $R_0 = 64$ and the ratio $E_1/E_0 = 100$ formed by large- and low-frequency elastic modulus. Zooms (not to scale!) into (b) contact geometry relative to the right crack tip located at x_{rc} and (c) interfacial stress relative to the left crack at x_{lc} . The elastic stress fields, defined as the equilibrium elastic stress for a fixed u(x), are shown for comparison in panel (c). The lateral coordinate x is normalized differently in different panels.

Table 1: List of most important symbols used in this letter.

$\Delta \gamma$	surface energy per unit area
$\mu_{ m T}$	Tabor parameter
$\sigma(x)$	stress field
$\sigma_{ m c}$	max. tensile stress of cohesive zone model
au	relaxation time
ω	angular frequency
$ ho_0$	flat-punch radius
$E(\omega)$	freqdep. Young's modulus
E_0, E_1	Young's mod. at low and high freq.
E^*	contact modulus
$F_{\rm p}(v)$	velocity-dependent pull-up force
$G_0, G(v)$	static and veldep. energy release rate
K	stress-intensity factor
R_0	radius of curvature of rigid indenter
V(g)	gap-dep. interaction potential per unit area
W, W(v)	(veldep.) work of separation
a_0, a_K	static and K -dep. crack tip radius
d	displacement of indenter
g, g(x)	(local) interfacial separation or gap
$g_{ m c}$	range of adhesion, or cut-off gap
q	wave number
$q_0, q_c(v)$	static and veldep. cut-off wave number
$q_{ m s}$	stiffness wave number
r	distance from crack tip
t	time
u(x)	displacement field
v	crack tip velocity
$v_{\mathbf{p}}$	pull-up velocity
. ()	(7)

over a meaningfully large parameter range. One purpose of this article is to fill this gap. A further, equally important question addressed here is how viscoelasticity affects the snap off in single-asperity contacts. This includes a

static and vel.-dep. cont. width at $\max(F_{\rm p})$

w, w(v)

test of the prediction [19,20] that fracture modes change from interfacial crack propagation to quasi-uniform bond breaking at small scales and an analysis of how the work of separation depends on the pull-off velocity.

Model. – The model studied in this work is depicted in fig. 2. It assumes a common, three-element viscoelastic solid, for which

$$\frac{E_0}{E(\omega)} = \frac{E_0}{E_1} + \left(1 - \frac{E_0}{E_1}\right) \frac{1}{1 - i\omega\tau}.$$
 (1)

Here, E_0 , $E(\omega)$, and E_1 are low-, arbitrary-, and high-frequency moduli, respectively, while τ is the relaxation time.

The interaction potential per unit surface area, V(g), associated with the contact formation is described by a recently proposed CZM [21], for which V(g) is zero if the gap g exceeds the cut-off gap g_c and

$$V(g) = -\Delta \gamma \times \begin{cases} \left[1 - (\pi g/g_{c})^{2}/2 \right], & \text{if } g < 0, \\ \left[1 + \cos(\pi g/g_{c}) \right]/2, & \text{if } 0 \le g < g_{c} \end{cases}$$
 (2)

otherwise. Here, $\Delta \gamma$ is the interfacial binding energy gained when cylinder and elastomer touch (g=0). The maximum tensile stress of our CZM is $\sigma_{\rm c} = \pi \Delta \gamma/(2\,g_{\rm c})$. An advantage of the employed CZM over commonly used Dugdale-type models is that ours is twice differentiable, as real interactions are, whereby numerical solutions of the dynamics are quite robust.

Simulations were conducted using a house-written Green's function molecular dynamics (GFMD) code, which has been described numerous times before, see, e.g., appendix 2 in ref. [22]. However, the used propagator was changed in order to reflect the dynamics of the standard three-element model leading to a similar approach as that pursued by Bugnicourt et al. [23]. To improve numerical stability, the interfacial stress and its time derivative, that

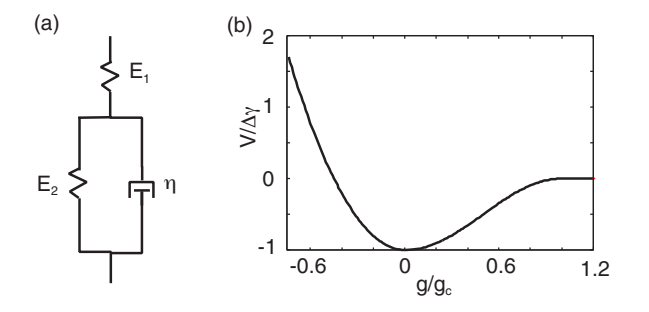


Fig. 2: (a) Three-element viscoelastic model. The high-frequency modulus $E_1 = E(\omega \to \infty)$ and the viscosity $\eta = 1/\tau$ are indicated. The low-frequency modulus follows from E_1 and E_2 according to $E_0 \equiv E(\omega = 0) = E_1 E_2/(E_1 + E_2)$. (b) The wall-wall interaction potential (per unit surface area) used in the numerical simulations.

is, the r.h.s. of eq. (4) in ref. [23], were low-pass filtered as described elsewhere [24]. For an alternative way of simulating the used viscoelastic model with GFMD, we refer to ref. [25].

The length of the periodically repeated simulation cell was generally set to $L = 4 R_0$, where the contact radius R_0 took the values $R_0 = 1, 8$, and 64. Note that three variables can be used to define the unit system. Throughout this work, we assume a unit system in which the contact modulus $E_0^* \equiv E_0/(1-\nu^2)$, τ , and the smallest R_0 define the units of stress, time, and length, respectively. Here, ν is the Poisson ratio, which is assumed to be independent of frequency. Real units can be produced by setting, e.g., $E_0^* = 5 \,\mathrm{MPa}, \ \gamma = 50 \,\mathrm{mJ/m^2}, \ \mathrm{in} \ \mathrm{which} \ \mathrm{case} \ \mathrm{the} \ \mathrm{unit} \ \mathrm{of}$ length would be 10 nm. From a continuum perspective, it might be more meaningful to state the Tabor parameter, which would read $\mu_{\rm T} = \sqrt[3]{R_0 \sigma_{\rm c}^3/(E_0^{*2} \Delta \gamma)}$, if the ratio $\Delta \gamma / \sigma_{\rm c}$ was used as the range of interaction in the common definition of $\mu_{\rm T}$. With our maximum tensile stress, $\sigma_{\rm c}$, the Tabor parameters realized in this study would range from $\mu_{\rm T} \approx 4$ for $R_0 = 1$ to $\mu_{\rm T} \approx 16$ for $R_0 = 64$, which could be classified as medium- to short-ranged adhesion. In comparison, Afferante and Violano studied effective surface energies in viscoelastic Hertzian contacts in the limit of long-range interaction, i.e., for $\mu_{\rm T} \approx 1/3.85$, and the fixed ratio $E_1/E_0 = 10$ in a compelling, recent study [18].

Throughout this manuscript, $E_0^* = 1$ and $\Delta \gamma = 0.01$. Moreover, space is always discretized into elements of length $\Delta x = 1/1024$. This motivated the peculiar value of $g_c = 0.0175156$, which was chosen as to make the maximum elastic stiffness, $\kappa_{\rm el}^{\rm max} \equiv \max(q) E_0^*/2$, i.e., the stiffness of the surface undulation with the largest wave number, exactly ten times the maximum curvature of V(g). As a consequence, the distance between the point of maximum tension and the points where the numerically determined static stresses or displacement fields closely approach their continuum solutions, be it inside or outside the contact, is also of order ten and even larger at high crack tip speeds. Due to such a fine discretization, lattice trapping is suppressed.

To further illuminate the model, fig. 1(a) shows the overall contact geometry and the stress field for a force-free static contact and panel (b) a zoom into the displacement field u(x) including our determination of the static crack tip radius $a_{\rm cr}$. Moreover, fig. 1(c) confirms that the interfacial stress $\sigma(x)$ in the vicinity of the crack tip obtained at different crack tip velocities v can be superimposed when scaling the distance from the crack tip with the ratio $q_c(v)/q_0$ deduced from eq. (3). For v=0, the elastic stress, $\sigma_{\rm el}(x)$ defined as the inverse Fourier transform of $qE_0^*\tilde{u}(q)/2$, superimposes with $\sigma(x)$. At intermediate $v, \sigma_{\rm el}(x)$ is still relatively close to $\sigma(x)$ in the immediate vicinity of the crack tip and approaches it asymptotically at large distances from the crack tip. However, elastic and interfacial stress fields differ substantially at large v. Since relaxation is driven by the difference between elastic and interfacial stress, dissipation occurs predominantly far away from the cracks in the latter case.

Theory. – In this section, we sketch the Persson-Brener theory [17]. The reader is referred to the original literature for a detailed derivation. In addition, we identify the analytical solution for the three-element model within the theory and discuss the relation between various useful length scales.

To quantify the viscous energy loss for a steadily moving crack, Persson and Brener [17] argued that the stress singularity near the crack tip is cut-off by the local maximum tension σ_c . This made them introduce a speed-dependent wave number cut-off $q_c(v)$, above which the elastomer no longer noticeably deforms. The cut-off reveals itself experimentally through a blunting of the crack tip at large crack tip speeds. It can be obtained through the self-consistent equation

$$q_{c}(v) = q_{0} \{1 - I(v q_{c}(v))\},$$
 (3)

where the static cut-off wave number $q_0 = q_c(0)$, whose relation to other characteristic distances and wave numbers is discussed at the end of this section, is the only adjustable parameter, and where

$$I(\omega) = \frac{2}{\pi} \int_0^1 dx \, \frac{\sqrt{1 - x^2}}{x} \operatorname{Im} \left\{ \frac{E_0}{E(x\omega)} \right\}. \tag{4}$$

From this, G(v), which turns out inversely proportional to $q_c(v)$, can be deduced through

$$G(v) q_c(v) = G_0 q_c(0).$$
 (5)

The imaginary part of $E^*/E(\omega)$ can be easily evaluated for the three-element model depicted in fig. 2 and the result be inserted into eq. (4) to yield the integral

$$I(\omega) = \left(1 - \frac{E_0}{E_1}\right) \frac{2}{\pi} \int_0^1 dx \sqrt{1 - x^2} \frac{\omega \tau}{1 + (\omega \tau x)^2}.$$
 (6)

It has the solution

$$I(\omega) = \left(1 - \frac{E_0}{E_1}\right) \frac{\sqrt{1 + (\omega \tau)^2} - 1}{\omega \tau}.$$
 (7)

As a consequence, the self-consistent equation to be solved for a standard, three-element half space becomes

$$\frac{q_{c}(v)}{q_{0}} = 1 - \left(1 - \frac{E_{0}}{E_{1}}\right) \frac{\sqrt{1 + q_{c}^{2}(v)v^{2}\tau^{2}} - 1}{q_{c}(v)v\tau}$$
(8)

after substituting $\omega = v q_{\rm c}(v)$. In principle, this is a quadratic equation in $q_{\rm c}(v)$ and therefore analytically solvable. However, the coefficients are cumbersome so we found a self-consistent solution of eq. (8) for $q_{\rm c}(v)$ to remain most convenient.

Quite a few characteristic distances or wavelengths and their corresponding wave numbers can be defined. Different distances and wavelengths should be generally related by conversion factors of order unity times $(2\pi)^{\pm 1}$. It may be beneficial to introduce them and to identify their mutual dependencies for our CZM defined in eq. (2). We expect the resulting conversion factors to be similar for other CZMs.

The first wave vector to be introduced is the one at which the stiffness $\kappa_{\rm el}(q) \equiv q E_0^*/2$ of a surface undulation with wave number q is equal to the maximum negative curvature of the interaction potential,

$$q_{\rm s} = 2 \max(-V''(g))/E_0^*.$$
 (9)

For our CZM, the term q_s , which we call stiffness wave number¹, can be calculated from $\max(-V''(g)) = (\pi/2)^2 \Delta \gamma/g_c^2$ and $\sigma_c = (\pi/2)\Delta \gamma/g_c$ so that

$$q_{\rm s} = \frac{2\,\sigma_{\rm c}^2}{E_0^*\,\Delta\gamma}.\tag{10}$$

Modes with wave numbers $q \ll q_{\rm s}$ will behave as in the continuum/short-range-adhesion limit, while those with $q \gg q_{\rm s}$ are too stiff to be distorted by the interfacial interactions. A motivated guess for the used conversion factor $\alpha_{\rm cs} \equiv q_{\rm c}/q_{\rm s}$ is provided further below.

We note in passing that eq. (9) is not directly applicable to CZMs for which the associated gap-dependent potential energy density V(g) is not twice differentiable or assumes a "funky" shape. Thus, the wave number cut-off q_c used in the Persson-Brener theory must be of order q_s . However, for conventional CZMs, like the Dugdale model, eq. (10) should be a good approximation.

Another characteristic length is the distance a_K from the crack tip beyond which the stress field approaches the asymptotic $\sigma(r) = K/\sqrt{2\pi r}$ relation, where K is the so-called stress-intensity factor. A convenient measure for a_K can be deduced from numerical data by realizing that the divergence of the stress for small r can be shielded with

$$\sigma(r) \approx \frac{\sigma_{\rm c} \sqrt{a_K}}{\left(r^2 + a_K^2\right)^{1/4}}.\tag{11}$$

This relation yields the correct $\sigma(r) = K/\sqrt{2\pi r}$ asymptotics for $r \gg a_K$, while turning $\sigma(0) = \sigma_c$ into a maximum. Data as that shown in fig. 1(c) gives a first estimate of $a_K \approx 0.4 \, a_{\rm s}$. Comparing this result to eq. (19) in ref. [17], it follows for the static stress-intensity factor that $a_K = a_0 \equiv 2\pi/q_{\rm c}(0)$, where a_0 is the static crack tip radius. However, for the simulation presented further below, we did not gauge a_0 on the static stress field. We found it more effective to set it such that it accurately reproduces the linear-response dissipation of the receding cylinder at extremely small velocities, which was achieved with the numerical value of $a_0 = 0.019$. This number is close to the shown crack tip radius of $a_{\rm cr} = 0.03$ and translates to $a_0 = 1.95 \, a_{\rm s}$.

Results for cylinders. – Analytical results predict that the maximum tensile force, also called the pull-off force, $F_{\rm p}$, satisfies $F_{\rm p}=(27\,\pi\,G^2\,E_0^*\,R_0/16)^{1/3}$ [26–28]. Treating the breaking of the adhesive bonds between the solids as the propagation of an opening interfacial crack also at the moment of pull-off, we therefore expect

$$\frac{F_{\rm p}(v)}{F_{\rm p}(0)} = \left(\frac{G(v)}{G_0}\right)^{2/3},$$
 (12)

where v is the crack tip velocity at the moment when the normal force reaches its maximum. In fact, fig. 3 reveals close agreement between simulation and theory for how the pull-off force increases with pulling speed. The static pull-off forces, $F_{\rm p}(0)$, needed to accurately normalize $F_{\rm p}(v)$ were deduced from mass-weighted GFMD simulations [29] using very small $v_{\rm p}$. They deviated at most by 0.1% from the just-stated, quasi-static continuum expression for $F_{\rm p}$.

Persson-Brener theory (full lines in fig. 3) match within the numerical precision in the linear-response regime at small velocities. This linear-response regime arises as a consequence of how the modeler (or nature!) discretizes the elastic solid. For coarse discretization, lattice pinning occurs so that instabilities become unavoidable [30], which in turn lead to Coulomb friction. However, at fine discretization, the discretization points, or "atoms", move continuously at all times under adiabatic driving and Stokes damping arises automatically. Power-law scaling of the damping force would only be expected down to infinitesimal small velocities right at the critical point (in the absence of thermal noise) separating the Stokes from the Coulomb regime [31]. There will still be extended velocity regimes, in which sub-linear small-velocity corrections to either G(v) or F(v) arise even if G(v) - G(0) and thus F(v) - F(0) ultimately cross over to Stokes, whenever $1/\sqrt{r}$ stress singularity near crack tips extends down to small but not atomic scales. It can also be noticed that the transition between linear and non-linear velocity dependence occurs at a crack tip velocity of v = 0.1, which is the velocity above which the elastic stress starts to deviate appreciably from the interfacial stress, as is revealed in fig. 4(c).

The terms stiffness wave vector, and the corresponding stiffness distance $a_s = 2\pi/q_s$ may appear odd. However, due to the fact that the words characteristic, cohesive, contact, crack, critical, and cross-over all start with the letter c and three out of those six words even start with cr. the need for unconventional variable names arose.

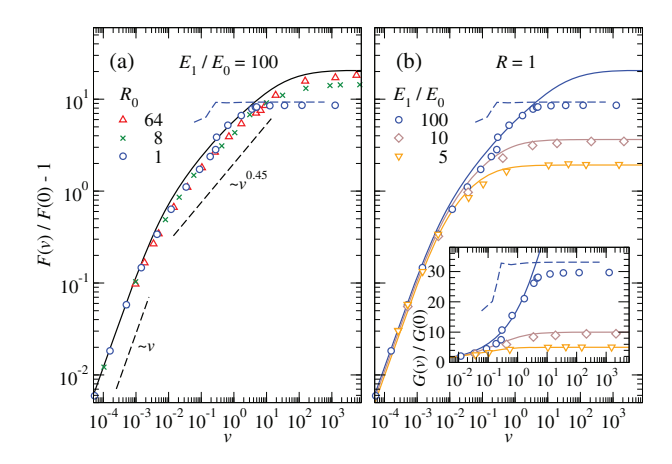


Fig. 3: Relative pull-off force increase, $F_{\rm p}(v)/F_{\rm p}(0)-1$, as a function of crack speed velocity v for (a) fixed $E_1/E_0=100$ and varying radius of curvature R_0 and (b) fixed $R_0=1$ and varying E_1/E_0 . Symbols and lines reflect simulation and theoretical results, respectively. Blue dashed lines reflect upper bounds to $F_{\rm p}$. The inset in panel (b) shows the ratio $G(v)/G_0$.

Differences between Persson-Brener theory and simulations reach 30% at intermediate velocities and decrease again for large tip radii at large v, where the viscoelastic fracture energy factor $G(v)/G_0$ plateaus close to the predicted value of E_1/E_0 . The latter ratio can be directly deduced from the theory by considering eq. (8) in the limit $v \to \infty$ and inserting the result, $q_c(v)/q_0 = E_0/E_1$, into eq. (5). A good agreement between theory and simulations is revealed particularly in the inset of fig. 3(b) for the two smaller E_1/E_0 ratios. This close match is an interesting result in its own right, also because the theory assumes steady-state crack propagation, while in reality, the crack tip speed is not constant at fixed pull-off velocity. Moreover, even better agreement must be expected for systems with a broad distribution of relaxation times, as the sharpwavenumber-cutoff approximation in the Persson-Brener approach should be most inaccurate for the three-element model with a single relaxation time.

Theory and simulation differ significantly in fig. 3 for small tip radii when v and E_1/E_0 are both large. This is due to the transition of the failure mode from crack propagation to quasi-uniform bond breaking, which was proposed to occur at small scales [19,20]. The argument for the phenomenon is that the tensile load in a finite contact should be roughly limited by the product of the maximum tensile stress and the contact width w. In fact, the dashed lines reflecting this estimate match the large-velocity limit for the $R_0 = 1$, $E_1/E_0 = 100$ system quite well if the value for w is the one observed in the simulations at the moment of maximum tensile force.

The suggested quasi-uniform bond breaking is also borne out from the displacement fields shown in fig. 4(a): at large v_p , the $R_0 = 64$ contact evidently fails by crack propagation while the displacement field moves almost homogeneously during failure for $R_0 = 1$. Specifically, for

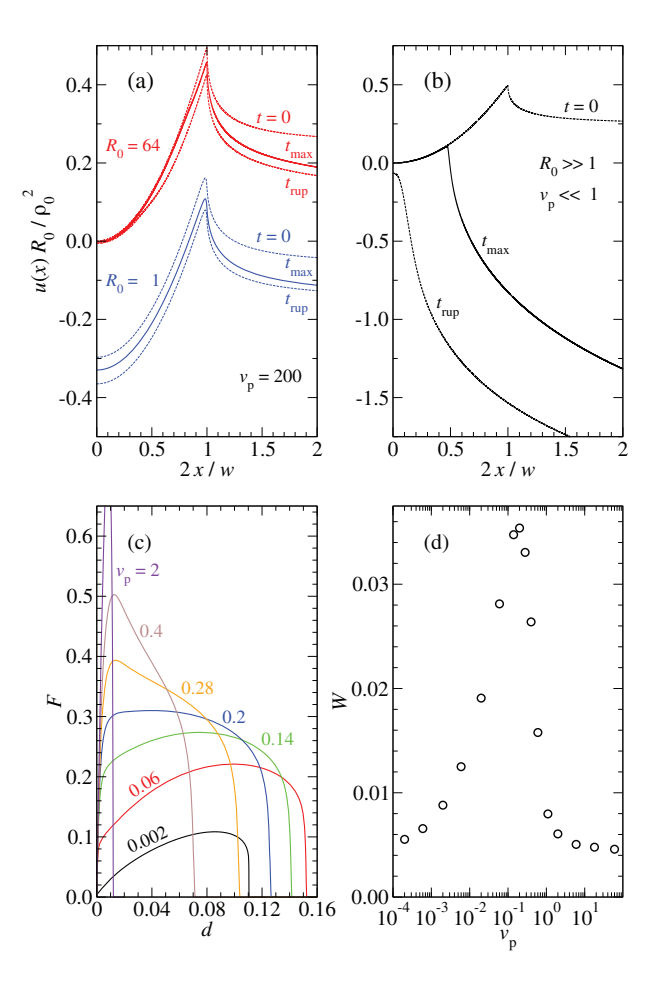


Fig. 4: (a) Displacement fields in static equilibrium at zero applied force (t=0), when the tensile force is maximum $(t=t_{\rm max})$, and at the moment of final rupture $t=t_{\rm rup}$ in the limit of large velocities for contact radii $R_0=64$ (red curves) and $R_0=1$ (blue curves). (b) Similar as (a) but for small pulling velocities and large R_0 . (c) Force-displacement curves at different velocities for the $R_0=1$ tip and (d) its velocity-dependent work of separation W.

 $R_0=1$, contact is already lost at r=0 when the tensile force reaches its maximum, while, for $R_0=64$, there is still contact near the origin directly after the moment of final rupture, which we define as the point in time right at which the tensile-load displacement curve assumes its most negative slope. At small velocities, all contacts studied here break in a similar way as shown for large R_0 in fig. 4(b). This is because the Tabor parameter is greater than unity even for $R_0=1$, i.e., $\mu_{\rm T}(R_0=1)\approx 4$ so that the adiabatic tip retraction is close to the short-range-adhesion continuum limit [32,33].

The blue, dashed lines in fig. 3 also reveal that the slope of the critical width w(v), defined as the width of the contact at the moment of maximum force, changes discontinuously at a certain crack tip velocity, which, however, is unrelated to the transition in the failure mode. Similar discontinuities in $\partial w(v)/\partial v$ occur for all investigated systems. As no theory apparently predicts this transition to

occur, all currently existing analytical approaches to the crack tip problem could be argued to be approximate.

To further illuminate the pull-off dynamics, fig. 4(c) shows various load displacement curves F(d) for $R_0=1$. Their shape changes indeed abruptly near $v_{\rm p}=0.2$, for which F(d) has a very flat maximum. At that pull-off velocity, $d_{\rm max}$ —the vertical distance moved to reach the maximum force— changes quite quickly from a value of order $d_{\rm max}(v\to 0)\approx 0.08$ by one decade to $d_{\rm max}(v\to \infty)\approx g_{\rm c}/2$, where the CZM assumes its maximum tensile stress.

Owing to the small forces needed to separate surfaces adiabatically and the small $d_{\rm max}$ needed to break the contact at large $v_{\rm p}$, the work of separation W turns out small in both limits. In between, viscous dissipation is largest leading to a pronounced maximum in W, which is shown in fig. 4(d). It can be said to arise, because a tensile force close to $F_{\rm p}(v\to\infty)/2$ acts over relatively large pulling distances.

Work of adhesion in selected two-dimensional contact problems. — Maxima in the work of separation at intermediate pulling velocities also occur for contact geometries other than cylinders, in particular for two-dimensional interfaces lacking the logarithmic system size corrections to W of line contacts. This will be discussed qualitatively for a flat, circular punch and numerically for a Hertzian contact.

For a flat punch with radius ρ_0 interacting through small-range adhesion, the contact area remains unchanged until the tensile force reaches its maximum, at which point an unstable crack starts propagating. For elastic solids, the force-distance relation reads $d = F/(2 \rho_0 E^*)$, while the pull-off force is given by $F_{\rm p} = \sqrt{8\pi E^* \Delta \gamma \rho_0^3}$. Thus, in the adiabatic case, the work of separation, W = $\int_0^{F_p} dF dF d(F) = 2\Delta \gamma$, does not depend on E^* . As a consequence, the result of this calculation does not change when replacing the low- with the high-frequency modulus so that W turns out identical in the limits $v \to 0$ and $v \to \infty$. Since W(v) evaluated at slightly positive v automatically exceeds W(0), there must be a maximum in the work of separation between the limits of infinitesimally small and infinitely large velocity. The correctness of this conclusion was validated numerically.

We also considered a Hertzian contact geometry. The system was modeled numerically with the following parameters: $R_0=1,~E^*=1,~\tau=1,~E_1/E_0=100,~\Delta\gamma=2\cdot 10^{-4},~g_{\rm c}=1.473\cdot 10^{-3}.$ With these choices, $\mu_{\rm T}\approx 2$. The pull-off force can be calculated with the well-known solution by Johnson-Kendall-Roberts (JKR) [34], which was also used to determine numerically the adiabatic work of separation for v=0. Results are shown in fig. 5.

As was the case for the cylinder, the work of separation is slightly enhanced for $v \to \infty$ compared to its adiabatic value W(0). At small velocities, we find an enhancement of both $F_{\rm p}$ and W(v), compared to their adiabatic values,

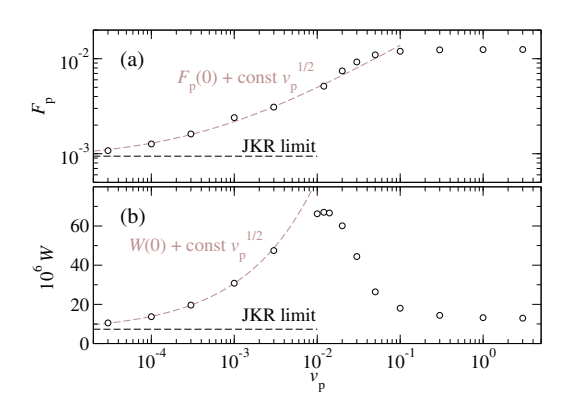


Fig. 5: (a) Pull-off force $F_{\rm p}$ and (b) work of separation W, both times as a function of pulling velocity $v_{\rm p}$ for a regular Hertzian tip. Adiabatic results from the JKR solution are included for comparison (dashed black lines) as well as fits (dashed brown lines).

which scales roughly with $\sqrt{v_{\rm p}}$. For these "two- plus one-dimensional" contacts, we did not manage to approach the linear response regime. Also note that the JKR limits will not be approached exactly for $v \to 0$, since the Tabor parameter of the investigated system was finite.

Discussion. — The maximum in the work of separation W might appear counterintuitive, since the entire initial contact area must be broken and the energy release rate G(v) increases monotonically with crack tip velocity v. However, the contact area at the moment of pull-off decreases with increasing pulling velocity. Near that moment, crack propagation becomes unstable and the viscoelastic-crack-propagation theory is not applicable, not even approximately. Breaking interfacial bonds no longer necessitates external energy supply.

Our calculation of the work of separation does not include the energy loss due to the (visco)elastic coupling between the center-of-mass mode of the elastomer's surface facing the indenter and its other surface, which is typically driven in laboratory experiments. However, only the work of separation due to finite q is dissipated in the vicinity of the contact so that we expect pull-off-induced near-surface heating to be largest at intermediate velocities. This effect should also hold for interfaces that are more complex than the one investigated in this work. For example, the product of maximum stress and the time during which nerves in the vicinity of hair roots are exposed to large forces should be maximal at intermediate pull-off velocities, which might explain the relatively large pain that is experienced when a bandage is pulled off at an intermediate velocity.

* * *

MHM acknowledges useful discussions with Sergey Sukhomlinov and Christian Müller.

REFERENCES

- [1] KNAUSS W. G., Int. J. Fract., 196 (2015) 99.
- [2] CRETON C. and CICCOTTI M., Rep. Prog. Phys., 79 (2016) 046601.
- [3] Gent A. N., Langmuir, 12 (1996) 4492.
- [4] Persson B. N. J., Albohr O., Heinrich G. and Ueba H., J. Phys.: Condens. Matter, 17 (2005) R1071.
- [5] VILLEY R., CRETON C., CORTET P.-P., DALBE M.-J., JET T., SAINTYVES B., SANTUCCI S., VANEL L., YARUSSO D. J. and CICCOTTI M., Soft Matter, 11 (2015) 3480
- [6] AFFERRANTE L. and CARBONE G., J. Mech. Phys. Solids, 96 (2016) 223.
- [7] HAN G., ERITEN M. and HENAK C. R., J. Mech. Behav. Biomed. Mater., 102 (2020) 103493.
- [8] SCHAPERY R. A., Int. J. Fract., 11 (1975) 141.
- [9] Schapery R. A., Int. J. Fract., 11 (1975) 369.
- [10] BARBER M., DONLEY J. and LANGER J. S., Phys. Rev. A, 40 (1989) 366.
- [11] HUI C.-Y., XU D.-B. and KRAMER E. J., J. Appl. Phys., 72 (1992) 3294.
- [12] HAIAT G., PHAN HUY M. C. and BARTHEL E., J. Mech. Phys. Solids, 51 (2003) 69.
- [13] Greenwood J. A., J. Phys. D, 37 (2004) 2557.
- [14] Greenwood J. A., J. Phys. D, 40 (2007) 1769.
- [15] DE GENNES P. G., Langmuir, 12 (1996) 4497.
- [16] FREUND L. B., Dynamic Fracture Mechanics (Cambridge University Press, Cambridge) 1998.
- [17] PERSSON B. N. J. and BRENER E. A., Phys. Rev. E, 71 (2005) 036123.

- [18] AFFERRANTE L. and VIOLANO G., J. Mech. Phys. Solids, 158 (2022) 104669.
- [19] Persson B. N. J., Wear, **254** (2003) 832.
- [20] GAO H. and YAO H., Proc. Natl. Acad. Sci. U.S.A., 101 (2004) 7851.
- [21] WANG A., ZHOU Y. and MÜSER M. H., Lubricants, 9 (2021) 17.
- [22] PRODANOV N., DAPP W. B. and MÜSER M. H., Tribol. Lett., 53 (2014) 433.
- [23] Bugnicourt R., Sainsot P., Lesaffre N. and Lubrecht A. A., *Tribol. Int.*, **113** (2017) 279.
- [24] SUKHOMLINOV SERGEY and MÜSER MARTIN H., Appl. Surf. Sci. Adv., 6 (2021) 100182.
- [25] VAN DOKKUM J. S. and NICOLA L., Model. Simul. Mater. Sci. Eng., 27 (2019) 075006.
- [26] Barquins M., J. Adhes., **26** (1988) 1.
- [27] CHAUDHURY M. K., WEAVER T., HUI C. Y. and KRAMER E. J., *J. Appl. Phys.*, **80** (1996) 30.
- [28] LIU T., JAGOTA A. and HUI C.-Y., Soft Matter, 11 (2015) 3844.
- [29] ZHOU Y., MOSELER M. and MÜSER M. H., Phys. Rev. B, 99 (2019) 144103.
- [30] HOLLAND D. and MARDER M., Phys. Rev. Lett., 80 (1998) 746.
- [31] MÜSER M. H., Phys. Rev. Lett., 89 (2002) 224301.
- [32] MAUGIS D., J. Colloid Interface Sci., 150 (1992) 243.
- [33] MÜSER M. H., Beilstein J. Nanotechnol., $\mathbf{5}$ (2014) 419.
- [34] JOHNSON K. L., KENDALL K. and ROBERTS A. D., Proc. R. Soc. A, 324 (1971) 301.